iScience

CellPress
OPEN ACCESS

Article

Phenotypic switching as a non-genetic mechanism of resistance predicts antibody therapy regimens

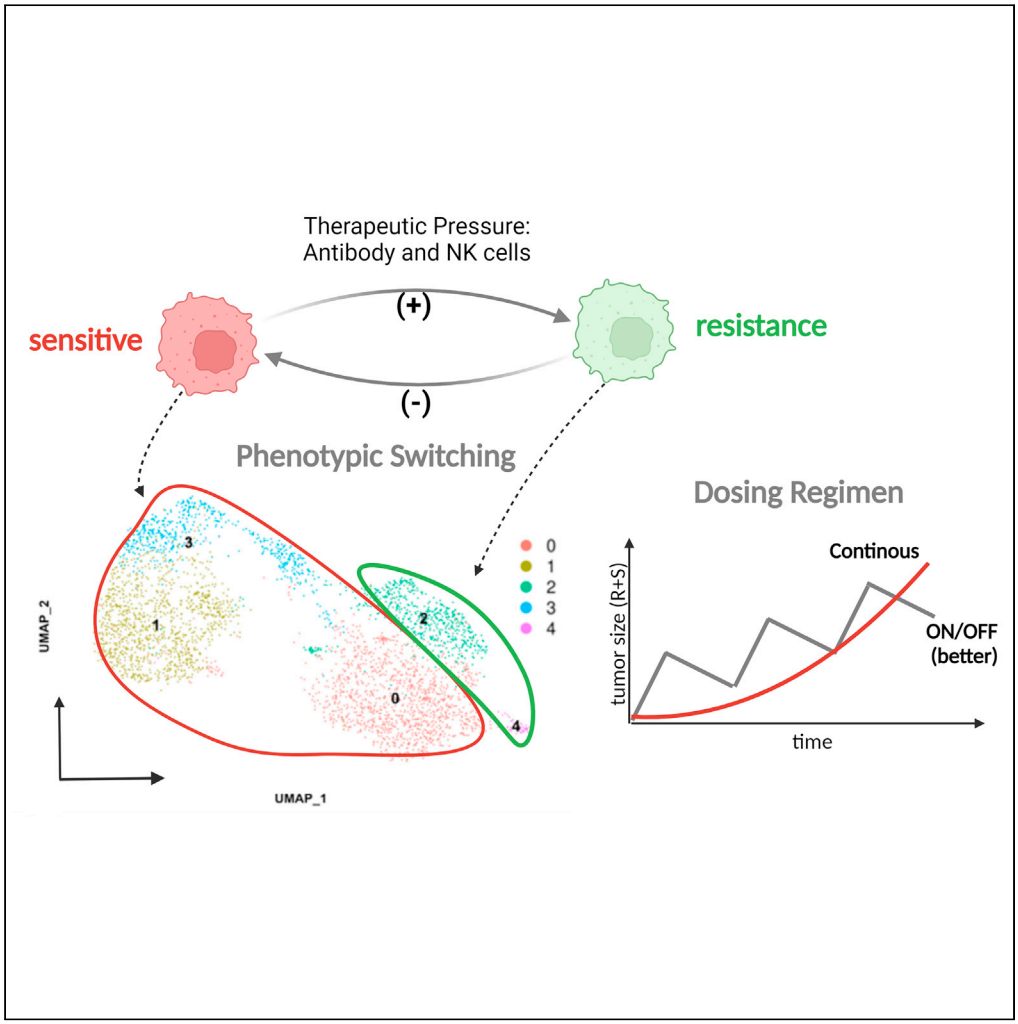

Jiawei Zhou, Can Liu, Yu Tang, Zhongbo Li, Yanguang Cao

yanguang@unc.edu

Highlights

Phenotypic switching drives non-genetic resistance to antibody therapy

Modeling these dynamics guides optimal dosing strategies

Intermittent dosing surpasses continuous regimens in delaying resistance

Zhou et al., iScience *27*, 109450
April 19, 2024
https://doi.org/10.1016/j.isci.2024.109450

iScience

CellPress
OPEN ACCESS

Article

Phenotypic switching as a non-genetic mechanism of resistance predicts antibody therapy regimens

Jiawei Zhou,[1] Can Liu,[1] Yu Tang,[1] Zhongbo Li,[2] and Yanguang Cao[1,3,4,*]

SUMMARY

Despite the specificity and effectiveness of antibody therapy, resistance to treatment remains a major barrier for their broad clinical applications. While genetic mutations are known to be critical, the impact of non-genetic mechanisms, such as epigenetic changes and phenotypic adaptations, on resistance to antibody-dependent cellular cytotoxicity (ADCC) is not fully understood. Our study investigated the non-genetic resistance mechanisms that colorectal cancer cells develop against cetuximab and the resulting ADCC pressure. Resistance clones exhibited decreased EGFR/HER2 expressions, enriched interferon-related pathways, and lower NK cell activation. Interestingly, these resistance clones regained sensitivity upon the withdrawal of therapeutic pressure, implying phenotypic plasticity and reversibility. To counter resistance, we developed a mathematical model recapitulating the phenotypic switching dynamics. The model predicted that intermittent dosing strategy outperforms continuous regimen in delaying treatment resistance. Our findings have implications for improving efficacy and circumventing resistance to targeted antibody therapies.

INTRODUCTION

The development of targeted antibody therapy has been a significant advancement in oncology treatment, which uses monoclonal antibodies to target specific proteins on the surface of cancer cells. These targeted agents seek to eradicate tumor cells by interfering with specific oncogenic molecules indispensable for tumor growth and progression, or initiating cell killing through activating effect cells, including antibody-dependent cellular cytotoxicity (ADCC) and antibody-dependent cellular phagocytosis.[1,2] In ADCC, antibodies bind to specific cell surface antigens expressed on cancer cells, such as the epidermal growth factor receptor (EGFR), and recruit immune cells, such as natural killer (NK) cells, to kill the cancer cells. Many antibody therapies, such as cetuximab, trastuzumab, and rituximab, rely on ADCC as a primary mechanism of action. Despite great therapeutic efficacy, resistance to antibody therapies remains prevalent, leading to treatment failure and disease relapse.[3–5]

Resistance to antibody-induced effector functions occur through both genetic and non-genetic mechanisms. While genetic mutations have long been recognized as a significant contributor to the development of resistance to targeted antibody therapies,[6,7] there is now increasing recognition that non-genetic mechanisms can also play a major role.[8,9] Non-genetic mechanisms of resistance or phenotypic adaptation can include the activation of alternative signaling pathways, changes in protein expression or glycosylation patterns, or alterations in the tumor microenvironment that limit antibody efficacy.[10–12] In the case of ADCC, cancer cells can develop resistance by downregulating the expression of target antigens or adhesion molecules, reducing the efficacy of immune cell-mediated killing.[13] Understanding the molecular mechanisms of resistance to ADCC and its reversibility is critical for developing treatment strategies to overcome it and improve the efficacy of antibody therapy in cancer treatment.

Phenotypic adaptation or switching, as a common non-generic mechanism of resistance, has emerged as an important reason for treatment failure in targeted antibody therapies.[14,15] It is becoming increasingly clear that phenotypic switching involves the reversible conversion of tumor cells to a different phenotype that is less susceptible to immune attack induced by therapeutic antibodies. Here we investigated the dynamics of phenotypic switching and the mechanisms underlying the resistance to cetuximab-initiated ADCC in colorectal cancer cells. Cetuximab is an EGFR-targeted monoclonal antibody for metastatic colorectal cancer (mCRC) that binds to the EGF receptors on the tumor cell surface and elicits tumor-killing effect through ADCC (Figure 1A).[16–21] Despite cetuximab showed great benefits in mCRC patients in clinical trials, many patients developed resistance after a transient response to the drug.[22,23] It has been well established that CRC cells with *KRAS/NRAS/BRAF* mutations exhibit genetic resistance to cetuximab.[22,24] Interestingly, recent clinical evidence indicated that tumors without genetic mutations can also acquire cetuximab resistance through non-genetic mechanisms.[25] Understanding and targeting non-genetic mechanisms of resistance is essential for improving the efficacy of targeted antibody therapies and overcoming resistance.

[1]Division of Pharmacotherapy and Experimental Therapeutics, School of Pharmacy, University of North Carolina at Chapel Hill, Chapel Hill, NC 27599, USA
[2]Division of Pharmacoengineering and Molecular Pharmaceutics, School of Pharmacy, University of North Carolina at Chapel Hill, Chapel Hill, NC 27599, USA
[3]Comprehensive Cancer Center, School of Medicine, University of North Carolina at Chapel Hill, Chapel Hill, NC 27599, USA
[4]Lead contact
*Correspondence: yanguang@unc.edu
https://doi.org/10.1016/j.isci.2024.109450

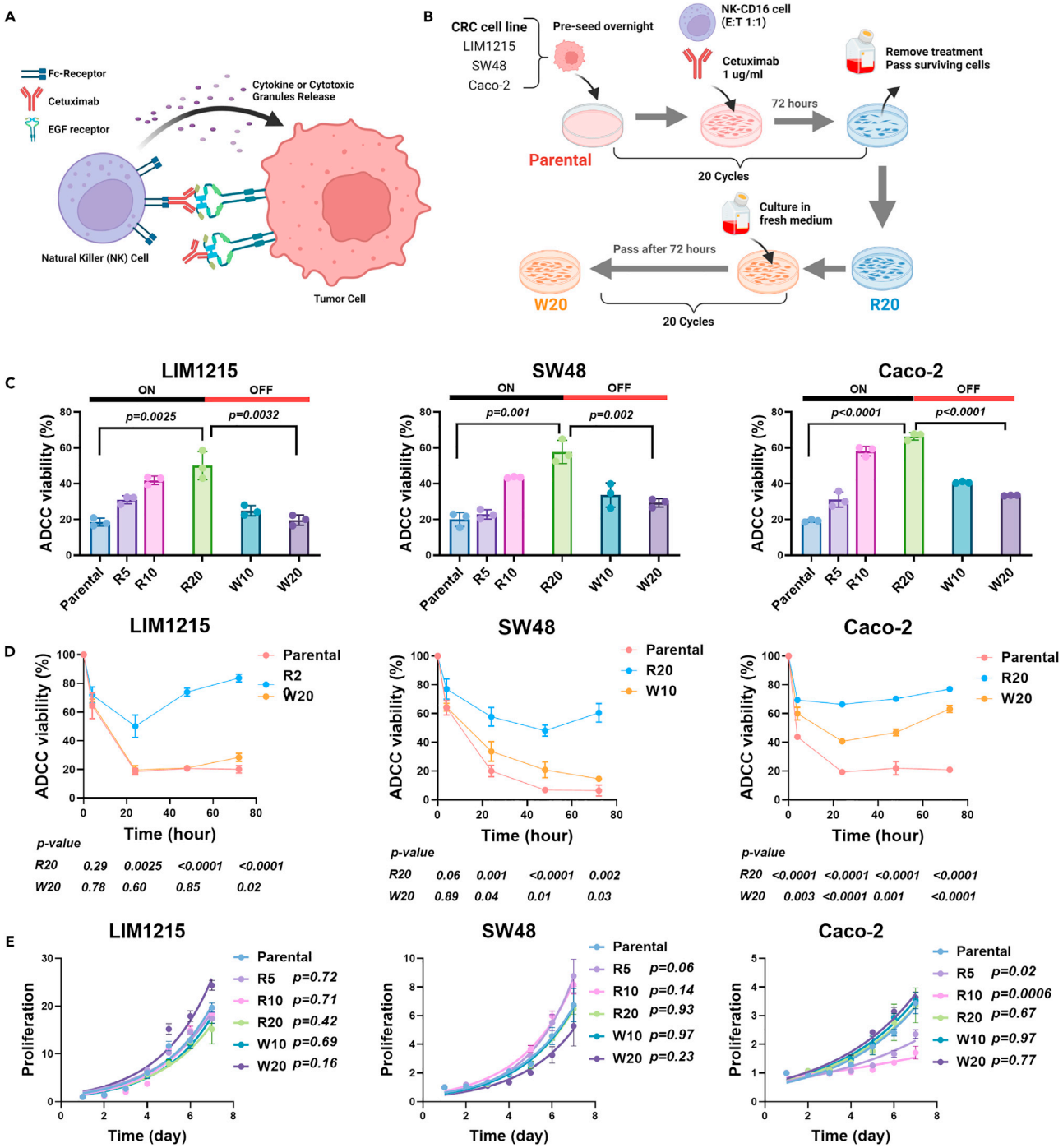

Figure 1. Phenotypic switching, a mechanism of resistance to ADCC, is largely reversible

(A) The schematic diagram of ADCC and related molecules.

(B) The workflow of generating ADCC-resistant and reversed clones using three colorectal cancer cell lines.

(C) ADCC viability (i.e., ADCC resistance degree) of generated clones across cell lines, including the parental, R5, R10, and R20 (clones after 5, 10, and 20 generations of ADCC challenge, n = 3), and W10, W20 (10 and 20 generations after washout of ADCC challenge, n = 3). Data are represented as mean ± SD.

(D) Clones ADCC viability in 72 h (n = 3). Statistical significance was compared with parental clones using unpaired t tests. Data are represented as mean ± SD.

(E) Cell proliferation measured in 7 days (n = 3). The solid lines are the fitted exponential cell growth curves. Statistical significance was compared with parental clone using generalized additive model. Data are represented as mean ± SD.

The development of strategies and treatment regimens that can target these phenotypic resistances and prevent their emergence represents a critical area of research in cancer therapy. In this study, we focused on elucidating the mechanisms, as well as the dynamics of phenotypic resistance to cetuximab-mediated ADCC in CRC cells and determined how we can capitalize on the phenotypic switching dynamics by developing treatment regimens with better tumor control. Through mathematical modeling, we found that using on-and-off dosing strategies for targeted antibody therapies, rather than continuous dosing, may lead to a better control of the resistant cell population and tumor growth. Understanding the dynamics of phenotypic switching informs treatment regimens that can capitalize on them, potentially leading to better tumor control and improved patient outcomes.

RESULTS

Phenotypic switching, a mechanism of resistance to ADCC, is largely reversible

Previous studies have shown that cetuximab-induced ADCC is correlated with EGFR expressions in CRC cell lines[26]; we, therefore, selected human CRC cell lines with high EGFR expression for deriving ADCC-resistant clones (LIM1215, SW48, and Caco-2). Tumor cells were started from a single clone and incubated under continuous ADCC pressure imposed by cetuximab (1 μg/mL) in the presence of NK-CD16 cells (E:T ratio 1:1). After 72 h of selection, surviving cells were collected and recovered in fresh medium for 1–7 days until confluence for next cycle of ADCC challenge. The cells were incubated for up to 20 cycles. We also investigated the reversibility of ADCC resistance by culturing the resistant clones in fresh medium without ADCC pressure for up to additional 20 generations (Figure 1B).

Cell viability was measured for parental, and clones after 5, 10, and 20 cycles of ADCC challenge and clones after 10 and 20 generations of washout were defined as R5, R10, R20, W10, and W20 clones. In all parental cells, up to 80% of tumor killing was observed at 24 h. Cell surviving fraction (or resistance) gradually increased over time. In the end, R20 clone had a significantly higher degree of ADCC resistance than parental clones in all cell clones (Figure 1C). ADCC viability of the washout clones (W10 and W20) became significantly lower than the resistant clones and got closer to the parental clones, indicating the reversibility of the ADCC resistance state in our *in vitro* system (Figure 1C). The degree of reversibility appears to be higher in LIM1215 than SW48 and Caco-2 cells. The temporal profiles during ADCC cycle also showed that LIM1215 cell had more complete reversibility with nearly full recovery of ADCC sensitivity, whereas Caco-2 cells only recovered 50% of ADCC sensitivity by the end of 20 generations of washout (Figure 1D).

Next, we compared the proliferation rates across cell clones. No significant difference in proliferation rates was observed between the parental and R20 or W20 in LIM1215 and SW48 cell clones (left and middle, Figure 1E), even though R10 clones showed a trend of higher proliferation and W20 showed a slightly lower proliferation than the parental SW48 cells. The proliferation of Caco-2 cell clones exhibited a nonlinear process, where two intermediate clones R5 and R10 experienced a drastic decline of proliferation from the parental while the proliferation rate of R20 was similar to the parental.

Overall, all cell lines used in the study developed resistance to ADCC induced by cetuximab after around 20 cycles of ADCC challenges. The resistance phenotype was largely reversible upon the withdrawal of ADCC pressure. These findings suggest that phenotypic switching is a critical non-generic mechanism of resistance to antibody-mediated cellular cytotoxicity.

Decreased membrane EGFR and increased HER2 expressions in ADCC-resistant clones

Tumor resistance to cetuximab may result from the decreased expression of the target protein EGFR.[26,27] We quantified the membrane expression levels of EGFR and HER2 in parental, R20, and W20 clones. In LIM1215 and SW48 cells, the EGFR expression significantly decreased in R20 clones compared to the parental clones, and the W20 clone had a comparable EGFR expression with the parental clone (Figure 2A), implying reversibility. Interestingly, in Caco-2 cells, the EGFR expression did not noticeably change with the resistance phenotypes, (Figure 2A), suggesting different resistance mechanism across cell type.

The decreased EGFR expression may lead to the compensatory increase in HER2 expression as a molecular mechanism of resistance, as shown in previous studies.[28,29] We found that HER2 expression was significantly increased in the R20 clones compared to parental and W20 clones in SW48 and Caco-2 cells but not in LIM1215 cells, suggesting the compensatory increase in HER2 as a mechanism of cetuximab resistance may not be consistent across all cell lines (Figure 2B).

Enriched IFN-response pathways and reduced NK activation in ADCC-resistant clones

We further assessed the differences between ADCC-resistant and -sensitive cell clones by examining their gene expression profiles. Specifically, in LIM1215 cells, we found that the R20 clone had distinct gene expression profiles compared to the parental and W20 clones (Figure 3A). Several genes were remarkably enriched in R20 compared to both parental and W20 clones, including HLA-DRA, CD74, and CCL3, while the HSPB1 gene was lost in R20 clones (Figure 3B). We performed GSEA analyses to explore the enriched gene pathways in ADCC-resistant cells, and found that IFN-associated pathways such as *IL2-STAT5* signaling, *IL6-JAK-STAT3*, IFN-α response, IFN-γ response, and *KRAS* signaling upregulation pathways were enriched in the R20 clones compared to the parental and W20 clones (Figure 3C). To further validate the overexpression of IFN-related pathways, we measured related protein expressions in LIM1215 parental, R20, and W20 clones. STAT1 and STAT3 were upregulated in R20 cells, while JAK2 and NF-κB p-65 were downregulated (Figure 3D). The original auto-western blot images were provided in Figure S1. These findings suggest that the overexpression of IFN-associated pathways may be involved in the resistance to ADCC.

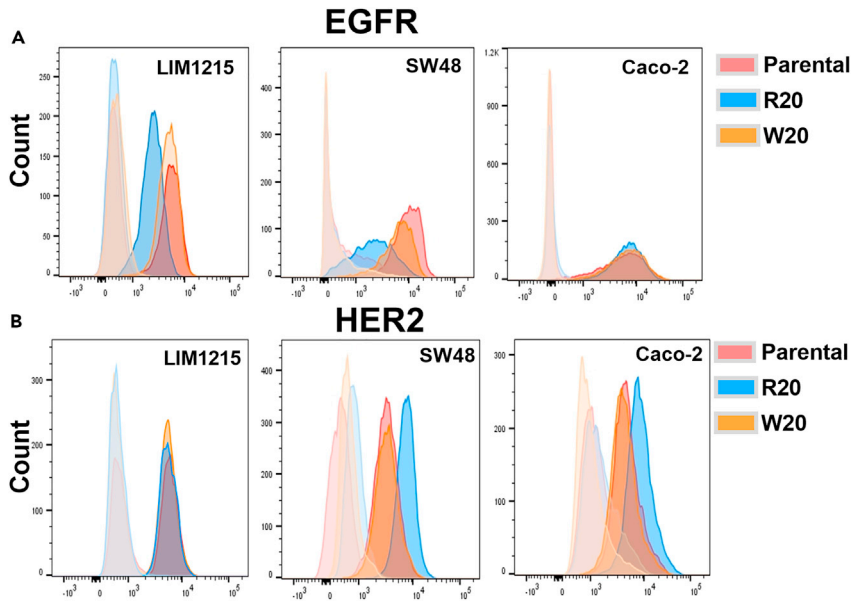

Figure 2. Decreased membrane EGFR and compensatory increased HER2 expressions across ADCC resistance state

(A and B) Flow cytometry analysis of EGFR (A) or HER2 (B) cell-surface expression in parental (red), R20 (blue), and W20 (orange) with isotype control expression for parental (light red), R20 (light blue), and W20 (light orange) in LIM1215, SW48, and Caco-2 cell lines.

We also found that IFN-related genes and pathways were similarly enriched in ADCC-resistant clones in SW48 and Caco-2 cells (Figures S2 and S3, respectively) cells, suggesting that overexpression of IFN-related genes is a key and common mechanisms in ADCC resistance across multiple CRC cell lines. Besides the IFN-related pathways, STAT-related pathways (IL2-STAT5 signaling, IL6-JAK-STAT3 signaling) and KRAS pathways were also upregulated in R20 clones compared to sensitive and W20 clones in all three cell lines (Figures 3C, S2C, and S3C).

IFN-γ is a cytokine that is produced by activated immune cells, and its secretion is an indicator of NK cell activation. To examine if defective cell-cell conjugation would contribute to the ADCC resistance, we measured the secreted IFN-γ by NK-CD16 cells in the medium 24 h after ADCC exposure. Three cell lines had different levels of NK cell activation, in which SW48 had the highest activation and Caco-2 had the lowest (Figure 3E). The degree of NK cell activation is inconsistent with their sensitivity to ADCC. Despite the difference in NK cell activation, all parental cell lines showed similar sensitivity to ADCC (Figures 1C and 1D). The R20 clone had significantly lower NK cell activation than the parental clones in all cell lines tested, suggesting that inefficient NK cell activation is involved in ADCC resistance. The W20 clones showed a partial restoration of the ability to activate NK cells, but still remained significantly lower than the parental clones, implying partial reversibility in their abilities for NK activation (Figure 3E).

From previous experiments, we observed that parental clone switched to ADCC-resistant state under continuous ADCC challenge, and ADCC-resistant R20 clone could recover sensitivity to some degree when ADCC condition was withdrawn. We compared the gene expression profiles in parental clone with W20. Although they had similar phenotypes, many gene expressions were significantly different for all three CRC cell lines (Figure S4). The transcriptomics heterogeneity between parental and W20 clones indicated that W20 clones were not fully reversed to parental state.

Phenotypic switching between cell subpopulations

To gain more insights into the cellular composition and mechanism underlying ADCC resistance, we conducted single-cell RNA sequencing analysis of LIM1215 parental, R20, and W20 clones. After filtering out low-viability cells, we identified 3,560 cells that classified into five cell clusters based on gene expression profiles (Figure 4A). The R20 clone exhibited upregulation of *CD74* and *HLA-DRA* genes, which were also upregulated in clusters 0, 1, and 3 (Figure 4B). Despite five distinct cell clusters, there were significant overlaps in clusters between phenotypes for each of the three cell clones (parental, R20, and W20). This suggests that there is a high degree of cellular heterogeneity within each phenotype, even though certain gene expression patterns in each cluster may be more associated with ADCC resistance.

The fractions of cell clones in each cluster were shown in Figure S5. The abundance of some clusters such as 1 and 3 increased in resistant clones, while some decreased such as 2 and 4. Although minimal difference was observed in the fraction of cluster 0 between parental and R20 clones, we detected upregulation of *CD74* and *HLA-DRA* genes in the R20 clone specifically within cluster 0 (Figure S6). This finding indicates that these cells undergo transcriptomic changes over time, ultimately leading to acquisition of resistance. For simplicity, we grouped five clusters into two subpopulations: *S* cells, which included clusters 2 and 4, and *R* cells, which originated from clusters 0, 1, and 3. The fraction of *S* cells was lowest in the R20 clone (9.8%), and similar in parental and W20 clones (23.9% and 16.9%, respectively) (Figure 4C). We found *R* cells

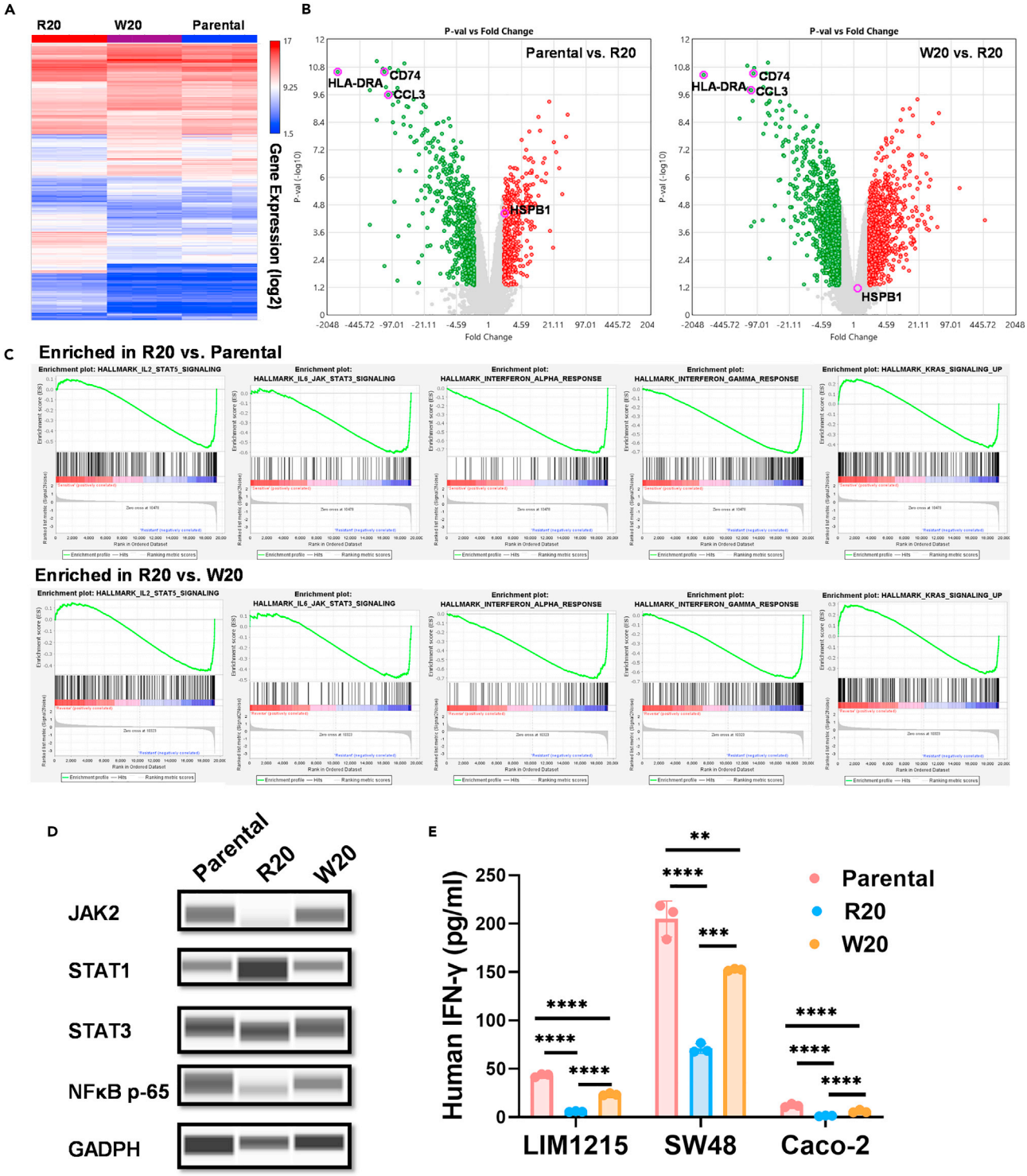

Figure 3. Resistance to ADCC is largely associated with enriched IFN-response pathways and reduced NK activation

(A) Heatmap of gene expression assessed by RNA sequence in LIM1215 parental, R20, and W20 cells. Differential gene expression analysis was conducted for genes possessing at least 2-fold changes and $p < 0.0001$. The heatmap is based on hierarchical clustering of all three cell subtypes (columns, triplicates for each cell subtype) and probes (rows) and contained 772 probes. Down- (blue) or up- (red) regulated expression is shown across each probe.

(B) Volcano plots of differential gene expression in parental vs. R20 (left) and W20 vs. R20 (right). The colored dots indicate the genes with p value <0.05 and gene-level fold change <-2 (green) or > -2 (red).

Figure 3. *Continued*

(C) Enrichment plots from GSEA for enriched pathways in R20 cells compared to parental (top) or W20 (bottom).

(D) Protein expression related to IFN-response pathways: JAK2, STAT1, STAT3, and NF-κB p-65 in LIM1215 parental, R20, and W20 cell clones.

(E) ELISA measured IFNγ levels released by NK cells in the media of parental, R20, and W20 cells under 24-h ADCC exposure for LIM1215, SW48, and Caco-2 cells (n = 3). Statistical significance was compared with parental clone using unpaired t tests. $p < 0.05$, *; $p < 0.01$, **; $p < 0.001$, ***; $p < 0.0001$, ****. Data are represented as mean ± SD.

had higher gene expressions with IFN-associated pathways, enrichment of DNA repair and helicase activity processes, which could potentially contribute to their ability to evade NK cell killing, as these processes are important for repairing DNA damage induced by NK cell-mediated cytotoxicity (Figure 4D). On the other hand, the enrichment of protein kinase activity processes in *S* cells may reflect their increased sensitivity to ADCC, as protein kinases play key roles in cell signaling pathways that regulate immune responses (Figure 4D). Further studies will be needed to investigate the functional significance of these gene expression changes in ADCC resistance and the potential therapeutic implications of targeting these pathways.

ADCC treatment decreased the fraction of *S* cells and increased the fraction of *R* cells, while withdrawal of treatment led to an increase in the fraction of *S* cells. Changes in the fraction of *S* and *R* cells in response to ADCC treatment suggest that the phenotypic switching between these two subpopulations is associated with ADCC resistance. Phenotypes are closely associated with the shift of cell subpopulations and the resistant phenotype is not fixed but rather dynamic and reversible. Understanding the mechanisms underlying this phenotypic switching may provide important insights into strategies for overcoming ADCC resistance in cancer therapy.

Phenotypic switching dynamics predicts effective dosing strategy

A mathematical model (Figure 5A) was developed to capture the phenotypic switching dynamics between *S* and *R* subpopulations, which was further validated with experimental data from LIM1215 parental, R20, and W20 clones (Figure 5B). Model parameters were outlined in Table 1, and it was found that the *R* population cell death rate under ADCC was lower in the R20 clone compared to parental and W20 clones. Resistance level evolves after 20 cycles of ADCC treatment and switches back when ADCC pressure is withdrawn. Overall, the model provided valuable insights into the dynamics of phenotypic switching and resistance in this system.

We further investigated the impact of different dosing regimens on *S* and *R* subpopulation by simulating the cell subpopulation switch under either continuous dosing (Figure 5C), 3 days on and 3 days off dosing (Figure 5D), 3 days on and 5 days off (Figure 5E), or 3 days on and 10 days off dosing (Figure 5F). Based on the simulation results, intermittent dosing strategies, such as 3 days on and 3 days off, 3 days on and 5 days off, and 3 days on and 10 days off, were found to delay final relapse by maintaining the phenotypic switching between S and R subpopulations. In contrast, continuous dosing initially showed benefits in controlling total tumor burden, but *R* subpopulations dominated and evolved, leading to later relapse.

Of note, the intermittent dosing strategies had lower accumulated doses compared to continuous dosing, while maintaining the phenotypic switching between *S* and *R* subpopulations. This allowed for a delay in the final relapse, which suggests that an on-and-off dosing strategy may be more favorable to prevent resistance evolution and prolong treatment efficacy while reducing potential dose-related toxicity. (Figure 5G)

Effective dosing strategy is highly dependent on the phenotypic switching dynamics

Phenotypic switching dynamics can vary between different cell lines and can have a significant impact on the effectiveness of cancer treatment. In this study, the LIM1215 cell line showed a relatively lower rate of resistance evolution but a rapid and nearly complete restoration of sensitivity after withdrawal of selection pressure compared to the Caco-2 cell line (Figures 1C and 1D). These differences in phenotypic switching dynamics suggest that different cell states may require different dosing strategies for optimal treatment efficacy.

We evaluated the impact of resistance evolution rate (w) and reversibility (μ_RS) on the effectiveness of intermediate dosing strategy depends on the specific dosing schedule employed. To begin with, we examined the total cell number at day 100 under continuous dosing versus 3 days on and 3 days off dosing, with varying resistance evolution rates (w). As expected, higher resistance evolution rates resulted in worse tumor control. Relatively speaking, at high resistance evolution rates, the 3 days on and 3 days off dosing strategy is more effective than continuous dosing, whereas for low resistance evolution rates, continuous dosing is more effective (Figure 6A). The length of the off period (3 days vs. 5 days) also has an impact, but this effect becomes minimal at high resistance evolution rates (Figure 6B).

The effectiveness of an intermittent dosing strategy is more pronounced than continuous dosing when the resistance to treatment is more reversible, i.e., high reversibility (μ_RS) (Figure 6C). This could be due to the fact that intermittent dosing allows for the switching between sensitive and resistant cell populations, which can prevent the development of resistance. Moreover, our simulation suggests that 3 days on and 3 days off dosing strategy is more effective than the 3 days on and 5 days off dosing strategy, even under varying resistance reversibility scenarios (Figure 6D).

DISCUSSION

While monoclonal antibody therapy has revolutionized cancer treatment, resistance to these therapies can develop and limit their clinical effectiveness.[30,31] Therapeutic antibodies against EGFR, such as cetuximab and panitumumab, are widely used to treat *KRAS* wild-type CRC patients.[32] Unfortunately, more than 65% of patients eventually develop resistance to these agents.[33] Most studies investigating

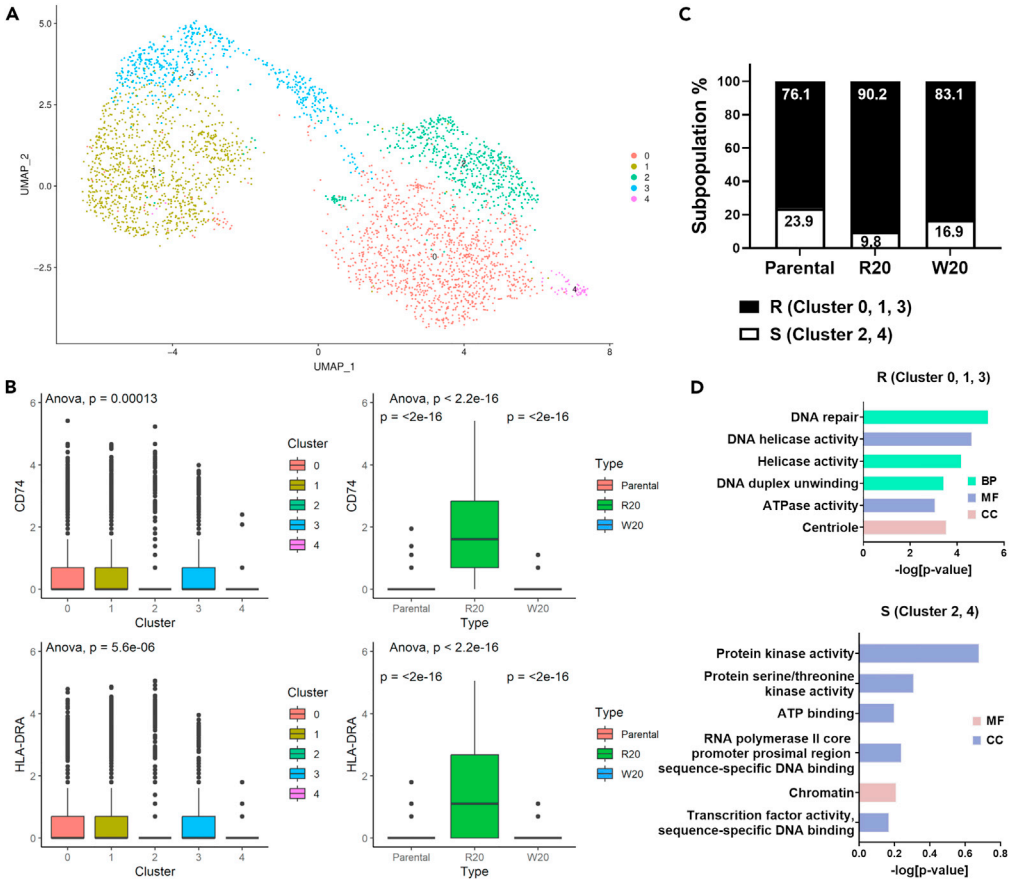

Figure 4. Gene expression at a single-cell RNA level and phenotypic switching among cell subpopulations

(A) UMAP projection of 3,560 LIM1215 cells (each point represents a single cell).

(B) CD74 and HLA-DRA gene expressions across UMAP clusters and types. Statistical significance was evaluated using ANOVA and unpaired t tests with state 0 or R20 clones as reference.

(C) The fraction of S (cluster 2, 4) and R (cluster 0, 1, 3) subpopulations in the parental, R20, and W20 cell clones.

(D) Top 50 upregulated GO pathways analyzed in the enriched genes expressed in R (top) or S (bottom) subpopulations. GO, gene ontology; BP, biological process; CC, cellular component; MF, molecular function.

cetuximab resistance focused on genomic mutations. In this context, the therapy acts as a selective pressure that favors the survival and growth of the cells carrying genetic mutations and creates more aggressive cell traits.[34] These resistant cells then become dominant in the tumor population, leading to disease progression and eventually treatment failure. This evolutionary process is driven by the principles of natural selection, where genetic or phenotypic variations that confer a survival advantage in the presence of the therapy are preferentially passed on to the next generation of cells. Emerging evidence suggests that non-genetic mechanisms, such as phenotypic switching, have been shown to play a role in the development of resistance to cetuximab and many other antibody-targeted therapies.

ADCC is an important mechanism of action for antibody therapies. Despite the effectiveness of ADCC, tumors can still develop mechanisms to evade the immune response initiated by antibody therapy. Multiple mechanisms of resistance to ADCC have been reported. However, the mechanisms of tumor cells developing resistance and escaping ADCC have not yet been completely clear. In this study, we investigated how tumor cells developed resistance to ADCC initiated by cetuximab through mechanisms of phenotypic switch. We initially generated multiple non-genetic ADCC-resistant CRC cells clones and then characterized the molecular characteristics underlying each phenotype, as well as model the dynamics of phenotypic switching for prediction of effective dosing strategy.

Our study has uncovered some important insights into the mechanisms of ADCC resistance in CRC cells. We found that the resistant phenotype is transient, and the fact that cells can restore ADCC sensitivity when treatment is withdrawn is particularly intriguing. Despite differences across cell lines, ADCC-resistant phenotypes generally involved the downregulation of EGFR and compensatory increase of HER2, as well as alterations in the IFN-related gene pathway and reduced NK cell activations. ADCC-resistant cells also had increased expressions in antigen-presenting and immune synapse formation-related genes like HLA-DRA, CD74, and CCL3 and reduced expressions in HSPB1, a known chaperone of EGFR.[35–38] Identification of five distinct cell clusters with different transcriptional profiles associated with these phenotypes is also an interesting finding. Even though it remains challenging to completely separate cell clusters across phenotypes, the changes in

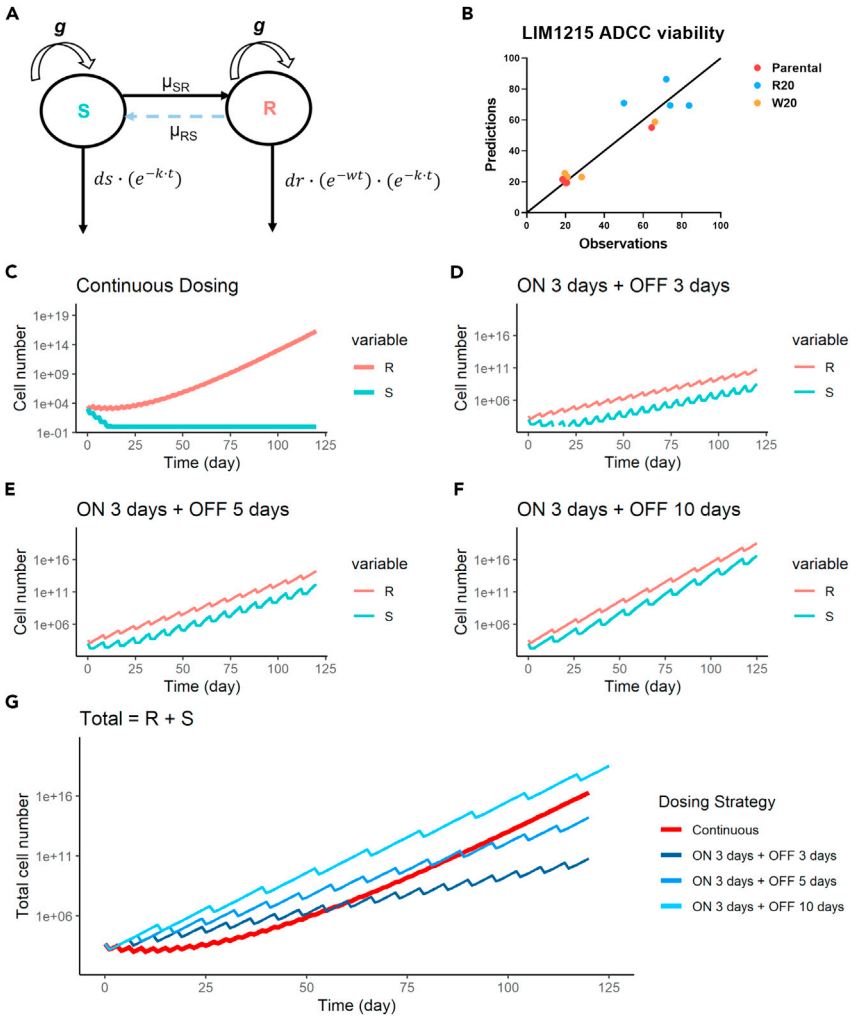

Figure 5. Simulated phenotypic switching dynamics predicts effective dosing strategy

Reversible resistance favors an intermediate dosing strategy for tumor containment.

(A) The model structure that describes phenotypic switching between two subpopulations.

(B) Model calibration using LIM1215 ADCC viability data.

(C) The growth dynamics of two cell subpopulations under continuous dosing strategy (3 days per cycle, 40 total doses). Simulated cell numbers below one was fixed to one in the plot.

(D) The growth dynamics of two cell subpopulations under 3 days on and 3 days off dosing strategy (20 total doses).

(E) The growth dynamics of two cell subpopulations under 3 days on and 5 days off dosing strategy (15 total doses).

(F) The growth dynamics of two cell subpopulations under 3 days on and 10 days off dosing strategy (10 total doses).

(G) The profiles of total tumor burden (*S* + *R*) vs. time under different dosing strategies.

cluster abundance were associated with alterations in cellular phenotypes, suggesting that phenotypic switching among cell subpopulations underlies the development of ADCC resistance in these cells. However, more validation experiments such as siRNA are needed to further explore the causative relationships between gene expression changes and ADCC resistance.

We took a simplistic approach to model the dynamics of phenotypic switching by assuming two cell subpopulations (*S* and *R*) at each phenotypic state and the fraction of these two subpopulations determines the level of tumor ADCC resistance. By simulating the changes in these subpopulations over time, we were able to predict the optimal dosing schedule that would minimize the emergence of resistant subpopulations and confer a durable control of tumor growth. The mathematical models suggested that continuous dosing of cetuximab would lead to rapid evolution of tumor cells to higher resistance levels, ultimately resulting in tumor relapse. However, by using intermittent treatment regimens, the resistant cells can be re-sensitized, and further phenotypic switching can be prevented. This information can be used to inform the development of more effective dosing strategies for cetuximab and other antibody therapies.

The potential benefits of intermittent therapy in cancer treatment have been found in previous published clinical studies. Adaptive therapy is an intermittent therapy strategy that limits the resistant subclones' growth using the sensitive subclones.[39] Different from traditional

Table 1. Model parameters

Parameter	Definition (Unit)	Value	Relative Standard Error (%)	Calculation
μ_SR	Transition rate from *S* to *R* when treatment is on (1/day)	0.347	944	Model estimation
μ_RS	Transition rate from *R* to *S* when treatment is off (1/day)	0.0014		Calculated from R20 and W20 *R* and *S* fraction
g	Cell growth rate (1/day)	0.4		Calculated from cell proliferation data
ds	*S* death rate under treatment (1/day)	5	Fixed	Fixed per prior analysis
k	Efficacy decay rate (1/day)	2.67	17.7	Model estimation
dr – Parental	Parental clone *R* death rate under treatment (1/day)	4.26	21.1	Model estimation
dr – R20	R20 clone *R* death rate under treatment (1/day)	0.78	19.9	Model estimation
dr – W20	W20 clone *R* death rate under treatment (1/day)	3.76	75.7	Model estimation
W	Resistance evolution rate (1/day)	0.028		Calculated from *dr*-Parental and *dr*-R20

maximum tolerated dose regimens, adaptive therapy proposes a "drug vacation" to allow the sensitive cells to outgrow and inhibit drug-resistant cell expansion.[40] Clinical evidence showed that adaptive therapy successfully delayed tumor resistance and prolonged patient survival.[41,42]

Previous studies have suggested a trade-off between cell proliferation and drug tolerance. In some cases, tumor cells may enter a state of slow proliferation in order to survive treatment, which is similar to a process known as diapause in some organisms.[43,44] This state is thought to allow cells to conserve energy and avoid the toxic effects of cytotoxic and targeted therapies. One study, using an epidermoid carcinoma cell line A431, revealed a significantly lower growth rate in cetuximab-resistant clones than sensitive cells.[27] However, this trade-off between proliferation and drug tolerance may not be clearly evidenced in ADCC-resistant phenotypes, as different types of resistance mechanisms can arise in different cell types and under different treatment conditions. The lack of a decrease in proliferation rate in the ADCC-resistant state suggests that the mechanism underlying phenotypic switching in our study is probably not driven by an apparent trade-off between cell proliferation and drug tolerance. Instead, it may be driven by neutral non-genetic evolution, which means that the resistant cells do not need to reduce their proliferation rates to survive ADCC and can maintain their growth rate while switching to an ADCC-resistant phenotype.

In summary, our study provides important insights into the mechanisms of ADCC resistance in CRC cells and highlights the potential benefits of intermittent dosing strategies to delay or prevent resistance. The reversible nature of the resistance phenotype also suggests that treatment strategies that allow for treatment breaks may be beneficial. Overall, our findings have significant implications for the development of more effective treatment approaches for EGFR-targeting therapies, and may inform future studies on the mechanisms of resistance to other targeted antibody therapies.

Limitations of the study

Our model has limitations. First, we estimated resistance evolution rate *w* by comparing the death rate of R20 and parental cell population, assuming the evolution time is 60 days. However, the 60 days assumption could be biased by experimental uncertainty. Second, our model simulations are limited in terms of clinical application because the *R* populations were not successfully suppressed in all simulated treatment strategies. A combination therapy should be considered to better control both *R* and *S* population. Third, we did not consider ecological interactions like competition or cooperation[45] between *S* and *R* population due to the limitations in our experimental data. Finally, experimental validations are needed to confirm the benefits of intermittent therapy.

STAR★METHODS

Detailed methods are provided in the online version of this paper and include the following:

- KEY RESOURCES TABLE
- RESOURCE AVAILABILITY
  - Lead contact
  - Materials availability
  - Data and code availablity
- EXPERIMENTAL MODEL AND STUDY PARTICIPANT DETAILS
  - Cell lines and single clone cell culture

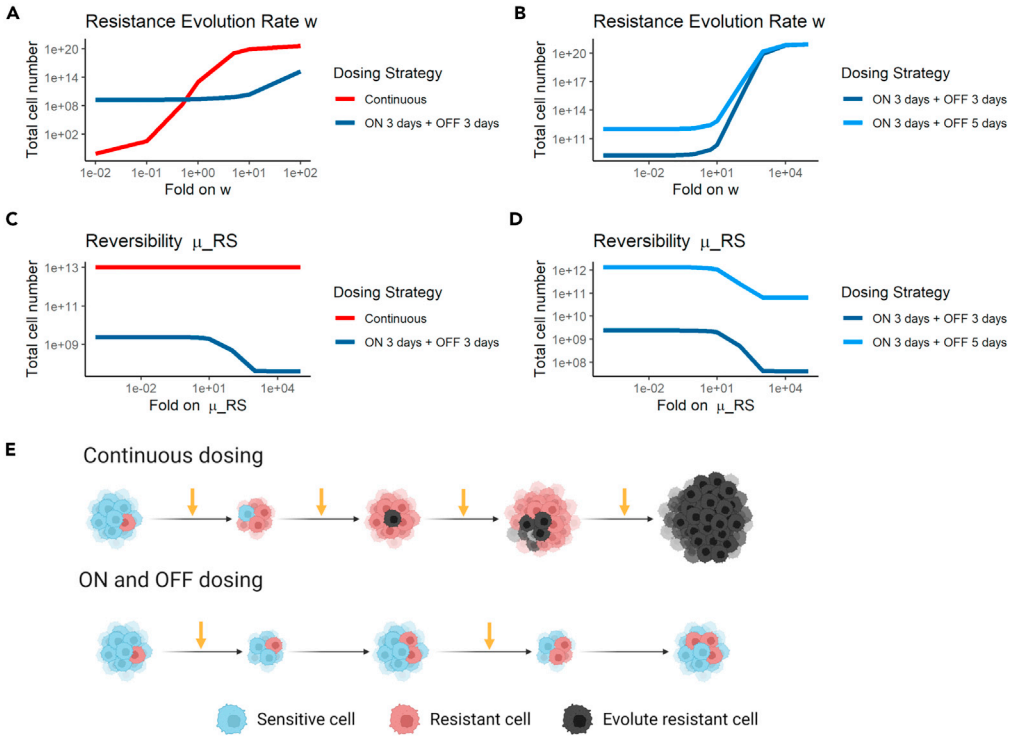

Figure 6. Effective dosing strategy is highly dependent on the simulated phenotypic switching dynamics

(A and B) The relationships between the total cell number at the end of 100 days of treatment and tumor resistance acquiring rate (*w*) under different dosing regimens: continuous vs. 3 days on and 3 days off dosing (A), and 3 days on and 3 days off vs. 3 days on and 5 days off dosing (B).

(C and D) The relationships between the total cell number at the end of 100 days of treatment and resistance reversibility rate (μ_RS) under different dosing regimens: continuous vs. 3 days on and 3 days off dosing (C), and 3 days on and 3 days off vs. 3 days on and 5 days off dosing strategy (D).

(E) The on-and-off dosing, compared to a continuous regimen, could capitalize on the reversibility of phenotypic resistance, and confer long-term containment of tumor.

SUPPLEMENTAL INFORMATION

Supplemental information can be found online at https://doi.org/10.1016/j.isci.2024.109450.

ACKNOWLEDGMENTS

We thank Mike Vernon from UNC Functional Genomics core for helping us perform bulk RNA sequencing experiments. We thank Carlton Anderson and Gabrielle Cannon from UNC Advanced Analytics core for helping us with single-cell RNA sequencing. We thank UNC Flow Cytometry core, UNC Bioinformatics core, and UNC High-Throughput Sequencing facilities for their support in this project. We thank Xiaozhi Liao from UNC School of Pharmacy DPET for helping us deposit sequencing data.

This work was funded by National Institute of General Medical Sciences, R35 GM152449.

AUTHOR CONTRIBUTIONS

Conceptualization, J.Z. and Y.C.; investigation, J.Z., C.L., and Y.T.; data curation, J.Z. and Z.L.; writing – original draft, J.Z. and Y.C.; review, C.L., Y.T., Z.L., and Y.C.

DECLARATION OF INTERESTS

The authors declare no conflicts of interest.

Received: April 25, 2023
Revised: January 28, 2024
Accepted: March 5, 2024
Published: March 7, 2024

REFERENCES

1. Ke, X., and Shen, L. (2017). Molecular targeted therapy of cancer: The progress and future prospect. Front. Lab. Med. *1*, 69–75.
2. Kaplon, H., and Reichert, J.M. (2021). Antibodies to watch in 2021. In MAbs (Taylor & Francis), pp. 1860476.
3. Gilad, Y., Gellerman, G., Lonard, D.M., and O'Malley, B.W. (2021). Drug Combination in Cancer Treatment—From Cocktails to Conjugated Combinations. Cancers *13*, 669.
4. Marusyk, A., Janiszewska, M., and Polyak, K. (2020). Intratumor heterogeneity: the rosetta stone of therapy resistance. Cancer Cell *37*, 471–484.
5. Whiting, F.J.H. (2021). Investigating the Evolutionary Dynamics of Drug Resistance in Colorectal Cancer Doctor of Philosophy.
6. Sforza, V., Martinelli, E., Ciardiello, F., Gambardella, V., Napolitano, S., Martini, G., Della Corte, C., Cardone, C., Ferrara, M.L., Reginelli, A., et al. (2016). Mechanisms of resistance to anti-epidermal growth factor receptor inhibitors in metastatic colorectal cancer. World J. Gastroenterol. *22*, 6345–6361.
7. Janjigian, Y.Y., Sanchez-Vega, F., Jonsson, P., Chatila, W.K., Hechtman, J.F., Ku, G.Y., Riches, J.C., Tuvy, Y., Kundra, R., Bouvier, N., et al. (2018). Genetic predictors of response to systemic therapy in esophagogastric cancergenomic biomarkers in esophagogastric adenocarcinoma. Cancer Discov. *8*, 49–58.
8. Huang, S. (2021). Reconciling Non-Genetic Plasticity with Somatic Evolution in Cancer. Trends Cancer *7*, 309–322. https://doi.org/10.1016/j.trecan.2020.12.007.
9. Cahill, D.P., Kinzler, K.W., Vogelstein, B., and Lengauer, C. (1999). Genetic instability and darwinian selection in tumours. Trends Cell Biol. *9*, M57–M60.
10. Black, J.R.M., and McGranahan, N. (2021). Genetic and non-genetic clonal diversity in cancer evolution. Nat. Rev. Cancer *21*, 379–392.
11. Hinohara, K., Wu, H.-J., Vigneau, S., McDonald, T.O., Igarashi, K.J., Yamamoto, K.N., Madsen, T., Fassl, A., Egri, S.B., Papanastasiou, M., et al. (2018). KDM5 histone demethylase activity links cellular transcriptomic heterogeneity to therapeutic resistance. Cancer Cell *34*, 939–953.e9.
12. Cavalli, F.M.G., Remke, M., Rampasek, L., Peacock, J., Shih, D.J.H., Luu, B., Garzia, L., Torchia, J., Nor, C., Morrissy, A.S., et al. (2017). Intertumoral heterogeneity within medulloblastoma subgroups. Cancer Cell *31*, 737–754.e6.
13. Pento, J.T. (2017). Monoclonal antibodies for the treatment of cancer. Anticancer Res. *37*, 5935–5939.
14. Shen, S., and Clairambault, J. (2020). Cell plasticity in cancer cell populations. F1000Res. *9*, 635.
15. Gunnarsson, E.B., De, S., Leder, K., and Foo, J. (2020). Understanding the role of phenotypic switching in cancer drug resistance. J. Theor. Biol. *490*, 110162.
16. Kurai, J., Chikumi, H., Hashimoto, K., Yamaguchi, K., Yamasaki, A., Sako, T., Touge, H., Makino, H., Takata, M., Miyata, M., et al. (2007). Antibody-dependent cellular cytotoxicity mediated by cetuximab against lung cancer cell lines. Clin. Cancer Res. *13*, 1552–1561. https://doi.org/10.1158/1078-0432.CCR-06-1726.
17. Kimura, H., Sakai, K., Arao, T., Shimoyama, T., Tamura, T., and Nishio, K. (2007). Antibody-dependent cellular cytotoxicity of cetuximab against tumor cells with wild-type or mutant epidermal growth factor receptor. Cancer Sci. *98*, 1275–1280.
18. Vincenzi, B., Schiavon, G., Silletta, M., Santini, D., and Tonini, G. (2008). The biological properties of cetuximab. Crit. Rev. Oncol. Hematol. *68*, 93–106.
19. Wang, W., Erbe, A.K., Hank, J.A., Morris, Z.S., and Sondel, P.M. (2015). NK cell-mediated antibody-dependent cellular cytotoxicity in cancer immunotherapy. Front. Immunol. *6*, 368.
20. Niu, Y.-X., Xu, Z.-X., Yu, L.-F., Lu, Y.-P., Wang, Y., Wu, C., Hou, Y.-B., Li, J.-N., Huang, S., Song, X., et al. (2022). Advances of research of Fc-fusion protein that activate NK cells for tumor immunotherapy. Int. Immunopharmacol. *109*, 108783.
21. Charles, W.Z., Faries, C.R., Street, Y.T., Flowers, L.S., and McNaughton, B. (2022). Antibody-Recruitment as a Therapeutic Strategy: A Brief History and Recent Advances. ChemBioChem. *23*, e202200092.
22. Zhao, B., Wang, L., Qiu, H., Zhang, M., Sun, L., Peng, P., Yu, Q., and Yuan, X. (2017). Mechanisms of resistance to anti-EGFR therapy in colorectal cancer. Oncotarget *8*, 3980–4000.
23. Van Emburgh, B.O., Sartore-Bianchi, A., Di Nicolantonio, F., Siena, S., and Bardelli, A. (2014). Acquired resistance to EGFR-targeted therapies in colorectal cancer. Mol. Oncol. *8*, 1084–1094.
24. Misale, S., Yaeger, R., Hobor, S., Scala, E., Janakiraman, M., Liska, D., Valtorta, E., Schiavo, R., Buscarino, M., Siravegna, G., et al. (2012). Emergence of KRAS mutations and acquired resistance to anti-EGFR therapy in colorectal cancer. Nature *486*, 532–536.
25. Santini, D., Vincenzi, B., Addeo, R., Garufi, C., Masi, G., Scartozzi, M., Mancuso, A., Frezza, A.M., Venditti, O., Imperatori, M., et al. (2012). Cetuximab rechallenge in metastatic colorectal cancer patients: how to come away from acquired resistance? Ann. Oncol. *23*, 2313–2318.
26. Seo, Y., Ishii, Y., Ochiai, H., Fukuda, K., Akimoto, S., Hayashida, T., Okabayashi, K., Tsuruta, M., Hasegawa, H., and Kitagawa, Y. (2014). Cetuximab-mediated ADCC activity is correlated with the cell surface expression level of EGFR but not with the KRAS/BRAF mutational status in colorectal cancer. Oncol. Rep. *31*, 2115–2122.
27. Aldeghaither, D.S., Zahavi, D.J., Murray, J.C., Fertig, E.J., Graham, G.T., Zhang, Y.-W., O'Connell, A., Ma, J., Jablonski, S.A., and Weiner, L.M. (2019). A mechanism of resistance to antibody-targeted immune attack. Cancer Immunol. Res. *7*, 230–243.
28. De Pauw, I., Lardon, F., Van den Bossche, J., Baysal, H., Pauwels, P., Peeters, M., Vermorken, J.B., and Wouters, A. (2019). Overcoming intrinsic and acquired cetuximab resistance in RAS wild-type colorectal cancer: An in vitro study on the expression of HER receptors and the potential of afatinib. Cancers *11*, 98.
29. De Pauw, I., Lardon, F., Van den Bossche, J., Baysal, H., Fransen, E., Deschoolmeester, V., Pauwels, P., Peeters, M., Vermorken, J.B., and Wouters, A. (2018). Simultaneous targeting of EGFR, HER 2, and HER 4 by afatinib overcomes intrinsic and acquired cetuximab resistance in head and neck squamous cell carcinoma cell lines. Mol. Oncol. *12*, 830–854.
30. Weiner, L.M., Surana, R., and Wang, S. (2010). Monoclonal antibodies: versatile platforms for cancer immunotherapy. Nat. Rev. Immunol. *10*, 317–327.
31. Beck, A., Wurch, T., Bailly, C., and Corvaia, N. (2010). Strategies and challenges for the next generation of therapeutic antibodies. Nat. Rev. Immunol. *10*, 345–352.
32. Nakadate, Y., Kodera, Y., Kitamura, Y., Shirasawa, S., Tachibana, T., Tamura, T., and Koizumi, F. (2014). KRAS mutation confers resistance to antibody-dependent cellular cytotoxicity of cetuximab against human colorectal cancer cells. Int. J. Cancer *134*, 2146–2155. https://doi.org/10.1002/ijc.28550.
33. Allegra, C.J., Jessup, J.M., Somerfield, M.R., Hamilton, S.R., Hammond, E.H., Hayes, D.F., McAllister, P.K., Morton, R.F., and Schilsky, R.L. (2009). Testing for KRAS gene mutations

in patients with metastatic colorectal carcinoma to predict response to anti-epidermal growth factor receptor monoclonal antibody therapy. J. Clin. Oncol. *27*, 2091–2096.

34. Woolston, A., Barber, L.J., Griffiths, B., Pich, O., Lopez-Bigas, N., Matthews, N., Rao, S., Watkins, D., Chau, I., Starling, N., et al. (2021). Mutational signatures impact the evolution of anti-EGFR antibody resistance in colorectal cancer. Nat. Ecol. Evol. *5*, 1024–1032.
35. Choi, N.M., Majumder, P., and Boss, J.M. (2011). Regulation of major histocompatibility complex class II genes. Curr. Opin. Immunol. *23*, 81–87.
36. Su, H., Na, N., Zhang, X., and Zhao, Y. (2017). The biological function and significance of CD74 in immune diseases. Inflamm. Res. *66*, 209–216.
37. Maurer, M., and Von Stebut, E. (2004). Macrophage inflammatory protein-1. Int. J. Biochem. Cell Biol. *36*, 1882–1886.
38. Aldeghaither, D.S., Zahavi, D.J., Murray, J.C., Fertig, E.J., Graham, G.T., Zhang, Y.-W., O'Connell, A., Ma, J., Jablonski, S.A., and Weiner, L.M. (2019). A Mechanism of Resistance to Antibody-Targeted Immune Attack. Cancer Immunol. Res. *7*, 230–243. https://doi.org/10.1158/2326-6066.CIR-18-0266.
39. West, J., Ma, Y., and Newton, P.K. (2018). Capitalizing on competition: An evolutionary model of competitive release in metastatic castration resistant prostate cancer treatment. J. Theor. Biol. *455*, 249–260.
40. Gatenby, R.A., Silva, A.S., Gillies, R.J., and Frieden, B.R. (2009). Adaptive therapy. Cancer Res. *69*, 4894–4903.
41. Cunningham, J.J., Brown, J.S., Gatenby, R.A., and Staňková, K. (2018). Optimal control to develop therapeutic strategies for metastatic castrate resistant prostate cancer. J. Theor. Biol. *459*, 67–78.
42. Zhang, J., Cunningham, J.J., Brown, J.S., and Gatenby, R.A. (2017). Integrating evolutionary dynamics into treatment of metastatic castrate-resistant prostate cancer. Nat. Commun. *8*, 1816.
43. Rehman, S.K., Haynes, J., Collignon, E., Brown, K.R., Wang, Y., Nixon, A.M.L., Bruce, J.P., Wintersinger, J.A., Singh Mer, A., Lo, E.B.L., et al. (2021). Colorectal Cancer Cells Enter a Diapause-like DTP State to Survive Chemotherapy. Cell *184*, 226–242.e21. https://doi.org/10.1016/j.cell.2020.11.018.
44. Dhimolea, E., De, R., Simoes, M., Kansara, D., and Brown, M. (2021). An Embryonic Diapause-like Adaptation with Suppressed Myc Activity Enables Tumor Treatment Persistence. Cancer Cell *39*, 240–256.e11. https://doi.org/10.1016/j.ccell.2020.12.002.
45. Viossat, Y., and Noble, R. (2021). A theoretical analysis of tumour containment. Nat. Ecol. Evol. *5*, 826–835.
46. Sheffer, M., Lowry, E., Beelen, N., Borah, M., Amara, S.N.A., Mader, C.C., Roth, J.A., Tsherniak, A., Freeman, S.S., Dashevsky, O., et al. (2021). Genome-scale screens identify factors regulating tumor cell responses to natural killer cells. Nat. Genet. *53*, 1196–1206. https://doi.org/10.1038/s41588-021-00889-w.
47. Ryan, J.A. (2008). Cell cloning by serial dilution in 96 well plates protocol. https://www.corning.com/catalog/cls/documents/protocols/Single_cell_cloning_protocol.pdf.

STAR★METHODS

KEY RESOURCES TABLE

REAGENT or RESOURCE	SOURCE	IDENTIFIER
Antibodies		
cetuximab	MedChemExpress	Cat# HY-P9905
Human BD Fc Block	BD Biosciences	Cat# 564219
BV786 Mouse Anti-Human EGF Receptor	BD Biosciences	Cat# 742606
BV480 Mouse Anti-Human Her2/Neu	BD Biosciences	Cat# 746442
APC Mouse Anti-Human CD45	BD Biosciences	Cat# 555485
DAPI	BD Biosciences	Cat# 564907
BV786 Mouse IgG2b, κ Isotype Control	BD Biosciences	Cat# 564090
BV480 Mouse IgG1, k Isotype Control	BD Biosciences	Cat# 565652
TotalSeq-B hashtag antibodies	BioLegend	Cat# 394631
Chemicals, peptides, and recombinant proteins		
Hydrocortisone	Sigma-Aldrich	Cat# H6909
Human insulin solution	Sigma-Aldrich	Cat# I9278
Minimum Essential Medium Eagle	Sigma-Aldrich	Cat# M0644 -10X1L
Myo-Inositol	Sigma-Aldrich	Cat# I5125-50G
Folic acid	Sigma-Aldrich	Cat# F7876-25G
2-Mercaptoethanol	Sigma-Aldrich	Cat# M6250-100ML
Recombinant human Interleukin-2	PEPROTECH	Cat# 200-02
Y-27632	Sigma-Aldrich	Cat# 5.09228
Critical commercial assays		
Lonza Walkersville mycoplasma testing kit	Fisher	Cat# NC9725794
Lonza Walkersville controls for mycoplasma test	Fisher	Cat# NC9800365
Cell-Titer Glo cell viability assay	Promega	Cat# G9241
Cell-Titer Blue assay	Promega	Cat# PR-G8081
ELISA MAX™ Deluxe Set Human IFN-γ 5plates	Biolegend	Cat# 430104
RNeasy Plus Mini Kit	QIAGEN	Cat# 74134
Clariom™ S Array, human	ThermoFisher	Cat# 902926
GeneChip® WT PLUS Reagent Kit	Affymetrix	Cat# 902281
GeneTitan Hybridization Wash and Stain Kit for WT Arrays	Thermo Fisher	Cat# 901622
Deposited data		
Bulk RNA sequence data	This paper	GSE255674
Single-cell RNA sequence data	This paper	PRJNA1076459
Codes for modeling and simulations	This paper	https://github.com/zhoujw14/ADCC_model.git
Codes to process single-cell RNA sequence data	This paper	https://github.com/zhoujw14/ADCC_model.git
Experimental models: Cell lines		
LIM1215	Horizon Discovery, USA	HD116-Par
SW48	Horizon Discovery, USA	HD103-Par

(*Continued on next page*)

Continued

REAGENT or RESOURCE	SOURCE	IDENTIFIER
Caco-2	ATCC	ATCC® HTB-37
NK-CD16	ATCC	ATCC® PTA- 6967
Software and algorithms		
FlowJo (v10.8.0)	FlowJo, LLC	https://www.flowjo.com/solutions/flowjo/downloads
Compass for Simple Western	Simple Western™	https://www.bio-techne.com/resources/instrument-software-download-center/compass-software-simple-western
GeneChip Command Console Software (AGCC)	Thermo Fisher Scientific	https://www.thermofisher.com/us/en/home/life-science/microarray-analysis/microarray-analysis-instruments-software-services/microarray-analysis-software/affymetrix-genechip-command-console-software.html
Transcriptome Analysis Console v4.0	Thermo Fisher Scientific	https://www.thermofisher.com/us/en/home/life-science/microarray-analysis/microarray-analysis-instruments-software-services/microarray-analysis-software/affymetrix-transcriptome-analysis-console-software.html
Gene set enrichment analysis (GSEA)	UC San Diego and Broad Institute	https://www.gsea-msigdb.org/gsea/index.jsp
Database for Annotation, Visualization and Integrated Discovery (DAVID)	The Laboratory of Human Retrovirology and Immunoinformatics (LHRI: former LHR)	https://david.ncifcrf.gov/tools.jsp
bcl2fastq (v2.20.0)	Illumina	https://support.illumina.com/downloads/bcl2fastq-conversion-software-v2-20.html
CellRanger (v6.1.1)	10X Genomics	https://support.10xgenomics.com/single-cell-gene-expression/software/pipelines/latest/what-is-cell-ranger
Monolix 2023R1	Lixoft	https://lixoft.com/download/win64-monolix-suite-2023r1/
R 4.1.0	R Development Core Team	https://cran.r-project.org/bin/windows/base/old/4.1.0/
RStudio	Posit, PBC	https://posit.co/products/open-source/rstudio/
GraphPad Prism 9	GraphPad	https://www.graphpad.com/updates/prism-900-release-notes
Other		
LSRFortessa	BD Biosciences	https://www.bdbiosciences.com/en-us/products/instruments/flow-cytometers/research-cell-analyzers/bd-lsrfortessa
Cytation 3	BioTek	https://www.labwrench.com/equipment/14792/biotek-cytation-3-cell-imaging-multi-mode-reader
Bioanalyzer	Agilent	https://www.agilent.com/en/product/automated-electrophoresis/bioanalyzer-systems/bioanalyzer-instrument
Affymetrix GeneTitan MC Instrument	Thermo Fished Scientific	Cat# 00-0373
SH800Z cell sorter	Sony Biotechnologies	https://www.sonybiotechnology.com/us/instruments/sh800s-cell-sorter/
NovaSeq 6000 system	Illumina	https://www.illumina.com/systems/sequencing-platforms/novaseq.html

RESOURCE AVAILABILITY

Lead contact

Further information and requests for resources and reagents should be directed to and will be fulfilled by the lead contact, Yanguang Cao (yanguang@unc.edu).

Materials availability

This study did not generate new unique reagents. The parental, R20, and W20 clones of LIM1215, SW48, and Caco-2 cell lines are available upon request.

Data and code availablity

- Data: The bulk RNA sequence data in this study has been deposited to NCBI (GSE255674). The single-cell RNA sequence data in this study has been deposited to NCBI under BioProject PRJNA1076459.
- Codes: The codes to process sequencing data and the codes for mathematical modeling and simulations were deposited to Github. The link could be found in the key resources table.
- All other items: Any additional information required to reanalyze the data reported in this paper is available from the lead contact upon request.

EXPERIMENTAL MODEL AND STUDY PARTICIPANT DETAILS

Cell lines and single clone cell culture

The LIM1215 and SW48 cell lines were purchased from Horizon Discovery, USA. The Caco-2 cell line (ATCC HTB-37) was obtained from UNC Tissue Culture Facility. All three cell lines have been authenticated by gDNA and cDNA genotyping or STR profiling. LIM1215 cells were cultured in RPMI 1640 medium with L-glutamine, supplemented with 10% FBS, 1 μg/mL hydrocortisone, 1 μg/mL human insulin, 100 U/mL penicillin-streptomycin. SW48 cells were cultured in complete medium: RPMI 1640 medium with L-glutamine, supplemented with 10% FBS and 100U/mL penicillin-streptomycin. Caco-2 cells were cultured with Eagle's MEM, supplemented with 20% FBS and 100 U/mL penicillin-streptomycin. Human NK cell line was purchased from ATCC. NK cells were cultured based on the recipe from Dr. Garry Nolan Lab in α-MEM with deoxyribonucleosides and ribonucleosides, supplemented with 0.2 mM myo-inositol, 0.0625% folic acid, 10% FBS, 10% horse serum, 0.0001 M 2-mercaptoethanol, 2 mM L-glutamine, 1% non-essential amino acids, 1% Sodium-Pyruvate, 100 U/mL penicillin-streptomycin.

Human CRC cell lines were cultured from a single clone and passed every 3–5 days at 70–80% confluency. NK-CD16 cells were maintained in suspension and passaged every 2–3 days and stimulated with 100 IU/mL recombinant human Interleukin-2. All the cells were maintained at 37 °C in 5% CO_2 and tested negative for mycoplasma (Lonza Walkersville Mycoplasma Testing Kit). Cell counts were estimated by hemocytometer, and viable cells were identified by trypan blue. The freezing medium for LIM1215 and SW48 cells were 45% complete growth medium, 50% FBS, and 5% DMSO (Sigma). Caco-2 cells were frozen in complete growth medium supplemented with 5% DMSO. NK-CD 16 cells were frozen in 6% DMSO and 94% FBS.

METHOD DETAILS

ADCC assay

To examine cell viability under ADCC, Cell Titer Glow (CTG) viability assays (Promega) were conducted.[46] Cells were seeded at 5,000 cells/well in 50 μL growth medium in 96-well white clear-bottom plates with triplicates per experimental condition (control vs. ADCC). After overnight incubation, 10,000 NK-CD16 cells were added together with 1 μg/mL cetuximab in 50 μL tumor cell growth medium for ADCC; 50 μL growth medium was added for control. After 4-, 24-, 48-, and 72-h incubation, 20% CTG was added to each well. After 15 min incubation, the plates were read with a microplate reader (BioTek, Cytation 3). Cell viability was calculated as follows:

$$ADCC\ viability\ \% = 100\% \times \left(B_{sample} - B_{NK}\right)/B_{control} \quad \text{(Equation 1)}$$

where B_{sample} represents the bioluminescence signal measured in ADCC samples, B_{NK} represents the average bioluminescence signal measured in wells with only NK-CD 16 cells, and $B_{control}$ represents the bioluminescence signal measured in control tumor cells.

Cell proliferation

Tumor cells were plated at 1,000 cells/well in 100 μL growth medium in 96-well black clear-bottom plates at triplicates. Seven plates were prepared to measure proliferation across 7 days. CellTiter-Blue (Promega) assays were conducted per manufacturer's instructions for 7 days to measure cell fluorescence using microplate reader. Cell proliferation was normalized by the average fluorescence on day 1 and was fitted by an exponential model with least square objective function:

$$Flo = Flo0 \times \exp(k \cdot t) \quad \text{(Equation 2)}$$

where *Flo* is the measured fluorescence normalized by the baseline, *Flo0* is the initial state of the system, *k* is the proliferation rate constant, and *t* is the time. Cell growth rates were estimated in Graphpad Prism 9.

Flow cytometry

Cell clones were dissociated with 0.25% trypsin and then resuspended in growth medium, and aliquoted into flow tubes at 10^6 cell densities. Cells were then spun at 500xg for 5 min at 4 °C, and resuspended in 100 μL FACS buffer (2% FBS in PBS). To block non-specific binding of

antibodies to Fc receptors, 1 μL human Fc block (BD Biosciences) was added and incubated for 10 min at room temperature. Labeled antibodies were then added at the concentrations optimized by titration and incubated on ice for 20 min avoiding light. Samples were also stained with CD45 and DAPI to distinguish live tumor cells from NK-CD16 cells and dead cells. Samples were then washed with FACS buffer three times and resuspended in 500 μL FACS buffer. Flow antibodies and isotype controls were all purchased from BD Biosciences: EGFR (cat. no. 742606), HER2 (cat. no. 746442), CD45 (cat. no. 555485), DAPI (cat. no. 564907), IgG2b isotype control (cat. no. 564090), and IgG1 isotype control (cat. no. 565652). Samples were run in the University of North Carolina at Chapel Hill Flow Cytometry Core using LSRFortessa. Analyses were performed using FlowJo (v10.8.0).

Auto-western blot

Cell clones cultured in 10 cm dish were first rinsed with cold PBS, and then lysed with 500 μL RIPA buffer supplemented with 10 μL protease inhibitor. Lysate was put on ice for 20 min and vortexed every 5 min, and then centrifuged at 16,000 xg for 15 min. Clear lysates were collected and processed for auto western (RayBiotech, USA). Antibodies were provided by RayBiotech including JAK2, STAT1, STAT3, NF-κB p-65, and GADPH. Auto-western blotting images were processed using Compass for Simple Western software.

INF- γ ELISA assays

Cell clones were seeded in six-well plates (Fisher Scientific; cat. no. FB012927) at 250,000 cells/well and incubated in 2 mL growth medium overnight at 37 $^{\circ}C$ in 5% CO_2. The control wells were then exposed to culture medium only and the ADCC wells were incubated with 1 μg/mL cetuximab and 250,000 NK-CD16 cells (E:T ratio 1:1). After 24-h incubation, the medium was collected and spun down at 1,000 xg for 5 min. IFN-γ was detected in the supernatant using the ELISA MAX Deluxe Kit (BioLegend) according to the manufacturer's instructions.

Experimental Design (ADCC resistant cell lines)

Single clone was isolated for CRC cell line LIM1215, SW48, and Caco-2 by serial dilution in clear-bottom 96 well plates.[47] Parental human CRC cell lines cultured from single clone were seeded overnight in 10 cm dish at 10^6 cells per dish. The following day, 10^6 NK-CD16 cells with 1 μg/mL cetuximab (anti-EGFR) were added for ADCC challenge. The effector-to-target (E: T) ratio at the time of treatment addition equates to 1:1. After 72 h, we removed treatments by rinsing the dish with phosphate buffered saline (PBS). The remaining adherent cells were collected by trypsinization and recovered for 1–7 days until the cells were sufficient for next cycle of treatment. Identical conditions were used for each subsequent ADCC challenge. Over 4 months, 20 subsequent challenges were conducted. Cell ADCC viability was measured after 5, 10, and 20 cycles of challenges (R5, R10, and R20) to assess clone ADCC-resistance level. To test whether the derived ADCC-resistance is reversible or not, R20 clones were further cultured in fresh medium for another 20 cycles without ADCC pressure. The cell ADCC viability after 10 and 20 cycles of passage (W10, W20) was measured. Parental clones were maintained as control simultaneously. Parental, R5, R10, R20, W10, and W20 clones were expanded for one passage and cryopreserved (Figure 1B).

Bulk RNA sequence and gene-expression analyses

Triplicates of parental, R20, and W20 clones in all three tumor cell lines were collected using trypsin. RNA was then isolated from cell pellets using RNeasy Plus Mini Kit (QIAGEN) following the instructions. RNA concentrations were measured using Nanodrop (Thermo One C) and diluted to 83.3 ng/μL for sequencing. RNA quality was assessed by Bioanalyzer (Agilent) for an RNA Integrity Number (RIN) > 9. Sample preparations were followed by the WT PLUS Reagent Kit Manual (Thermo Fisher). Briefly, the GeneChip WT PLUS Reagent Kit (Affymetrix) was used to generate sense-strand cDNA from total RNA (250 ng). Then the cDNA was fragmented and labeled with the kit and was used to prepare a hybridization cocktail with the GeneTitan Hybridization Wash and Stain Kit for WT Arrays (Thermo Fisher). Processed cDNA was then hybridized to the Human HT Clariom S 24-peg plate arrays, washed, stained and scanned by the Affymetrix GeneTitan MC Instrument. GeneChip Command Console Software (AGCC) was used for GeneTitan Instrument control.

RNA sequence data of parental, R20, and W20 clones were analyzed using Transcriptome Analysis Console software v4.0 for each cell line, respectively. Data were initially processed with log2 variance stabilization and quantile normalization. Probes with false discovery rate p values below 0.01 and fold change >2 or < −2 were called statistically significant. The differentially expressed genes with p value <0.0001 were included in heatmap plots. Gene set enrichment analysis (GSEA) was performed using RNA sequencing data comparing R20 vs. parental and R20 vs. W20. The pathways enriched in R20 clones for all three tumor cell lines were reported.

Single-cell RNA sequencing

LIM1215 parental, R20, and W20 clones were collected by trypsinization, and washed with PBS supplemented with 2% FBS. Triplicates were prepared for each clone (~10^6 cells), and stained with CD45, DAPI, and TotalSeq-B hashtag antibodies (BioLegend) on ice for 20 min, avoiding light. Cells were then washed three times and resuspended in 500 μL growth medium supplemented with 1 μL Y-27632 and 10% FBS. Cells were sorted and isolated using the University of North Carolina at Chapel Hill Advanced Analytics Core's SH800Z cell sorter (Sony Biotechnologies).

Samples were prepared as outlined in the 10x Genomics Chromium Single Cell 3′ Reagent Kits User Guide (v3.1 chemistry) with Feature Barcording technology for Cell Surface Protein. After sorting, sample viability and concentration were assessed using a combination of acridine orange and propidium idodide via a LUNA-FL dual fluorescence automatic cell counter (Logos Biosystems). Following counting, the

appropriate volume of each sample was combined to produce a single pool containing approximately 20,000 cells from each treatment group. Samples with a cell concentration below that required for a target capture of 10,000 cells were pelleted and re-suspended in a reduced volume, then counted again prior to pooling and loading on a 10x Genomics Chromium Next GEM Chip G. After droplet generation, reverse transcription was performed and cDNA was recovered using the Recovery Agent provided by 10x Genomics. Purified cDNA was amplified for 12 cycles before being cleaned up and run on a Bioanalyzer (Agilent Technologies) to determine cDNA concentration. cDNA libraries were prepared with appropriate modifications to the PCR cycles per manufacturer's instructions. Samples of each library were pooled in an equimolar fashion and normalized to a concentration of 4 nM. The sample preparations were performed by the University of North Carolina at Chapel Hill Advanced Analytics Core.

The pooled samples were diluted to their final loading concentration and sequenced on a NovaSeq 6000 system (Illumina) with a minimum sequencing depth or 20,000 read pairs per cell and the following run parameters: read 1–28 cycles, read 2–91 cycles, index 1–8 cycles. Sequencing was performed by the University of North Carolina at Chapel Hill High-Throughput Sequencing Facility.

Raw sequencing data (bcl files) were converted to fastq files with Illumina bcl2fastq (v2.20.0) and aligned to human genome reference sequence. The CellRanger (v6.1.1) analysis pipeline was used to generate a digital gene expression matrix from this data. The raw digital gene expression matrix was filtered, centered log-transformed, normalized and clustered using R-4.1.0 and Rstudio. Cells with a very small library size (<1,000) and low RNA features (<500) were removed. Selection of a clinically relevant number of clusters was based on differential expression between neighboring clusters. Clusters were visualized using Uniform Manifold Approximation and Projection (UMAP). Genes identified enriched in R20 clones from RNA sequence experiments were compared across clusters and clones in single-cell RNA sequence data to further classify cell subpopulations. Top 50 expressed genes in each cell subpopulation were analyzed for Gene Ontology (GO) pathway using DAVID online tool. Clustering was performed using standard Seurat package procedures. Figures were generated in R-4.1.0 and Rstudio or Graphpad Prism 9.

Modeling the dynamics of phenotypic switching

A mathematical model was developed to describe the dynamics of phenotypic adaptation in cell subpopulations on- and off-treatment. The model assumed two cell subpopulations, S is the sensitive population, and R is the resistant population. Cell proliferation rate g was calculated from cell proliferation experiment. When the treatment is on, S could acquire resistance and switch to R at a rate of μ_SR. Cytotoxic effects on S and R are $ds(t)$ and $dr(t)$ and the efficacy declines at a rate of k because of declining function of effector cells. The degree of resistance evolves under selective pressure at rate w. The equations were shown in Equations 3 and 4.

$$\frac{dS}{dt} = g\cdot S - \mu\_SR\cdot S - ds\cdot e^{-k\cdot t}\cdot S \quad S(0) = f\cdot N \qquad \text{(Equation 3)}$$

$$\frac{dR}{dt} = g\cdot R + \mu\_SR\cdot S - dr\cdot e^{-w\cdot t}\cdot e^{-k\cdot t}\cdot R \quad R(0) = (1-f)\cdot N \qquad \text{(Equation 4)}$$

When the treatment is off, R gradually switch back to S at a rate of μ_RS. The model equations are shown in Equations 5 and 6.

$$\frac{dS}{dt} = g\cdot S + \mu\_RS\cdot R \quad S(0) = f\cdot N \qquad \text{(Equation 5)}$$

$$\frac{dR}{dt} = g\cdot R - \mu_{RS}\cdot R \quad R(0) = (1-f)\cdot N \qquad \text{(Equation 6)}$$

Where f is the fraction of S population in the cells measured from single-cell RNA experiment, and N is the initial total cell number.

Parameter μ_RS was estimated by fitting S cell fraction data in parental and R20 clones in Monolix 2023R1 Lixoft. Parameters μ_SR, dr, k, were estimated by fitting the LIM1215 ADCC viability data in 72 h in Monolix 2023R1 Lixoft, and parameter ds were fixed in the model estimation. Parental, R20, and W20 clones were estimated with different dr in the model and resistance evolution rate parameter w was calculated from the estimated dr in parental and R20 clones in Equation 7.

$$dr(R20) = dr(Parental)\cdot e^{-w\cdot t}, t = 60\ days \qquad \text{(Equation 7)}$$

Model simulations were performed in R 4.1.0 and RStudio using deSolve package.

Model parameters uncertainty and sensitivity

In the model development process, we initially estimated all the parameters. Notably, parameters ds and μ_SR exhibited substantial uncertainty, as indicated by large relative standard errors. This uncertainty was attributed to the inherent sparsity of the dataset. To address this issue and improve the precision of model parameters, we fixed parameter ds to our prior estimate in the final model.

Additionally, we conducted a local sensitivity analysis to evaluate the impact of the model parameters with high uncertainty (μ_SR and ds). Specifically, we simulated parameters (μ_SR and ds) within a range of 80%–120% of their estimates to assess potential shifts in tumor growth dynamics (Figure S7). The results indicated that parameter μ_SR and ds had minimal impact on tumor dynamics. Therefore, we fixed ds at a

value of 5, close to the prior estimate. This strategy, coupled with further model refinement, resulted in a final model characterized by reasonable parameter uncertainty.

QUANTIFICATION AND STATISTICAL ANALYSIS

Statistical analyses in ADCC viability and IFN-γ release comparisons were performed by unpaired t tests. Statistical analyses in cell proliferation were performed by generalized additive model including cell subtypes, time with a model of spine, and their interactions as dependent variables. Statistical comparisons between gene expression levels were performed by ANOVA and unpaired t tests. For statistical tests are presented as asterisks, $p < 0.05$, *; $p < 0.01$, **; $p < 0.001$, ***; $p < 0.0001$, ****.